Chemical Kinetics and Reactive Species in Normal Saline Activated by a Surface Air Discharge

Zhi Chao Liu, Li Guo, Ding Xin Liu,* Ming Zhe Rong, Hai Lan Chen, Michael G. Kong*

Normal saline is a common biological solution which provides much better living environment for *Staphylococcus aureus* than deionized water, but the plasma-activated normal saline is found to have a stronger bactericidal effect than the plasma-activated deionized water. A model is developed for the explanation, from which various kinds of reactive chlorine/oxychlorine species (RCS), such as HClO, are found to be generated in the plasma-activated normal saline. The production pathways of RCS are elucidated, in which O_3 plays as an important intermediate species. Compared to the plasma-activated deionized water, the concentrations of reactive oxygen/nitrogen species are lower, but the bactericidal effect is higher, implying that the RCS play a crucial role for the sterilization.
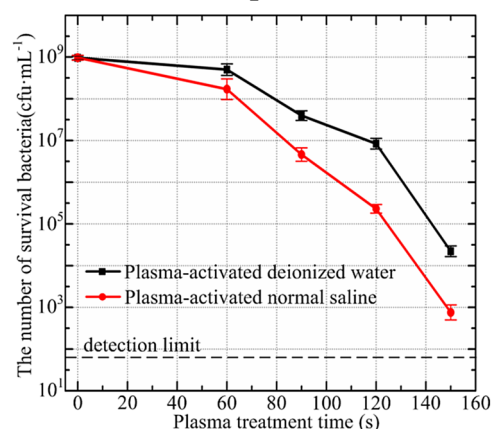
1. Introduction

Plasma-liquid interaction is a key link between the gas plasmas and the targets to be treated in water-rich substances, which is of great concern to various promising applications such as biomedicine,[1–3] sewage disposal,[4,5] and nano-technology.[6,7] Recent reports have witnessed great complexity of physicochemical processes in the plasma-liquid interaction, leading to a fundamental change of reactive species between the gas phase and the liquid phase.[8–12] The reactive species, especially reactive oxygen species (ROS) and reactive nitrogen species (RNS), are widely thought to play a dominant role in most applications,[13] but so far little has been known of their density correlations between the two adjacent phases.[14] This knowledge gap is a critical area in plasma science, which greatly hinders the future design and improvement of plasma sources for their intended applications.[15]

In this paper, the interaction between a surface air discharge and its downstream – normal saline was numerical studied. The numerical model was previously reported for the plasma treatment of deionized water.[16] And here, it was modified by adding 25 aqueous species

Prof. D. X. Liu, Prof. M. G. Kong, Dr. Z. C. . Liu, Prof. L. Guo, Prof. M. Z. Rong
State Key Lab of Electrical Insulation and Power Equipment, Center for Plasma Biomedicine, Xi'an Jiaotong University, Shaanxi, P R China
E-mail: liudingxin@mail.xjtu.edu.cn
E-mail: mglin5g@gmail.com
Prof. H. L. Chen, Prof. M. G. Kong
Frank Reidy Center for Bioelectrics, Old Dominion University, Norfolk, Virginia 23508, USA
Prof. M. G. Kong
Department of Electrical and Computer Engineering, Old Dominion University, Norfolk, Virginia 23529, USA

wileyonlinelibrary.com

originated in the plasma treatment of normal saline and their corresponding 96 aqueous reactions. Various chlorine/oxy-chlorine species were found to be generated as a result of the plasma treatment, and some of them were reported to have strong bactericidal effect.[17–19] For example, the minimum bactericidal concentration of HClO/ClO$^-$ for *Staphylococcus aureus* is just 12.5 μM for 60 min treatment at room temperature, lower than that of H$_2$O$_2$ by ~1600-fold.[17] Here, the surface air discharge was experimentally proved to have the stronger bactericidal effect in normal saline than that in deionized water, which was a surprise at first glance because normal saline was a better living environment for bacteria. This might be attributed to the chlorine/oxy-chlorine species generated in the plasma-activated normal saline. In this paper, the chlorine/oxy-chlorine species, except for the non-reactive Cl$^-$, were named as reactive chlorine/oxy-chlorine species (RCS). And their concentration distributions, as well as production mechanism in the plasma-activated normal saline, were discussed in details. The concentration distributions of ROS and RNS in the plasma-activated normal saline were also presented and compared with that in the plasma-activated deionized water. Based on these results, the effect of NaCl on aqueous ROS and RNS production was elucidated.

The paper is organized as follows: the experimental setup and the bactericidal effect are given in Section 2. The numerical model is briefly described in Section 3, and the simulation results are presented and discussed in Section 4. Concluding remarks are given in Section 5. The aqueous chemistry data for RCS is provided in the Supporting Information.

2. Experimental Setup and Its Bactericidal Effect

The experimental setup was previously detailed,[16,20] and is briefly described here. The surface discharge structure consists of three parts: a plane high-voltage (HV) electrode, a liquid-facing grounded mesh electrode, and a dielectric sheet sandwiched between the two electrodes (see Figure 1). When a sinusoidal high-voltage is applied to the HV electrode, plasmas are generated on the dielectric surface of the grounded electrode side. The surface plasmas are confined in the hexagon mesh elements with a good mesh-to-mesh homogeneity.[20] A petri dish (diameter = 3 cm) filled with deionized water or normal saline (the mass fraction of NaCl is 0.9%) is placed underneath the plasma source. And the air gap between the grounded electrode and the liquid level is fixed to be 1 cm by adjusting the thickness of the gaskets. The width of the surface plasma is much larger than 1 cm, which allows for one-dimensional
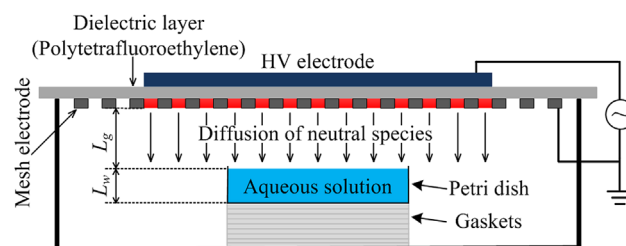
■ *Figure 1.* Schematic diagram of the experimental setup.

treatment in numerical simulation. The temperature of the mesh electrode measured with a thermocouple was found to remain roughly 300 K after 100 s of plasma treatment. The whole experimental system for plasma-liquid interaction is well sealed by a box made of polymethyl methacrylate (PMMA).

Normal saline is a common biological solution which generally provides a better living environment for cells/bacteria than deionized water. Is it still better for bacteria to survive after a plasma treatment? This question motivated us to compare the bactericidal effects in both aqueous solutions after plasma treatment, using the experimental setup shown in Figure 1. The conditions for this comparative study were carefully kept the same. The discharge power density was kept constant to be 0.2 W/cm^2, for which the voltage had a peak-to-peak value of 10 kV and a frequency of 50 kHz. The discharge voltage was lower than our previous report because the frequency was higher.[16] It should be noted that the power density used for simulation was 0.05 W/cm^2, four times lower than that for the experiments. The power density of 0.2 W/cm^2 was chosen for experiments, because in this case the bactericidal effect was pronounced when the plasma treatment time was just ~100 s. And for simulation the power density of 0.05 W/cm^2 was chosen to facilitate the comparison with our previous report on the plasma-activated deionized water.[16]

S. aureus N315 was chosen as the bacteria studied due to its high survival rate in deionized water, and it allowed for comparing with that in normal saline. An overnight culture of *S. aureus* was diluted 1:1000 in 150 ml Tryptone Soy Broth (TSB) medium and incubated with aeration at 250 r.p.m. at 37 °C until OD600 ~0.5. After that, the culture was centrifuged and washed with normal saline once, then resuspended in normal saline at OD600 ~2.0. Then, the aliquot of 1 ml *S. aureus* in normal saline was centrifuged, and the supernatant was discarded. The precipitated *S. aureus* was put into the plasma-activated solutions (deionized water and normal saline) which were just treated by the surface air discharge, and then incubated for 20 min at 22 °C. Serial dilutions were performed, and 10 μl of each dilution was spotted onto TSB agar plates. Plates were incubated overnight at 37 °C, and surviving cell numbers were counted by the spotting method. In order to

↖ Early View Publication; these are NOT the final page numbers, use DOI for citation !!

exclude untreated deionized water's effect on *S. aureus* N315, *S. aureus* N315 was incubated in the untreated deionized water for 1 h and the number of sterilization was less 10%, based on the results of three individual experiments. The surviving numbers of *S. aureus* after the treatment of both plasma-activated solutions are shown in Figure 2, on the plasma treatment time of 60, 90, 120, and 150 s. It can be seen that the surviving number reduces by 6 logs in the normal saline after 150 s of plasma treatment, indicating a very efficient bactericidal effect to achieve the sterility assurance level (SAL $\geq 10^6$). Interestingly, fewer numbers of *S. aureus* survive in the plasma-activated normal saline, implying that some strong bactericidal agents are generated therein, and these agents must not exist or have lower concentrations in the plasma-activated deionized water. Below we will discuss this using a modeling study.

3. Brief Description of the Model

The model was previously reported for the plasma treatment of deionized water,[16] and here it is modified by adding 25 aqueous species originated from NaCl and the corresponding 96 aqueous reactions (including 18 reversible reactions). All the species considered in the model are listed in Table 1. In the liquid region, the type of species in "deionized water" contains the aqueous species considered in the plasma-activated deionized water simulation,[16] and the type of species in "normal saline" contains the aqueous species considered in the plasma-activated normal saline simulation. The aqueous reactions for the reactive chlorine/oxy-chlorine species, as well as their rate coefficients, are provided in the Supporting Information.

The model consists of three modules for the plasma region, the air gap region, and the liquid region, and all of them are calculated simultaneously. A zero-dimensional module is used for the surface plasma in humid air, of which
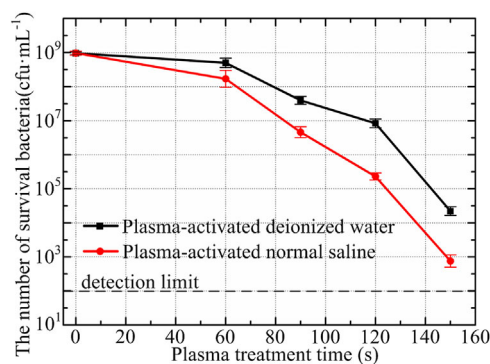
Figure 2. Comparison of the bactericidal effects between the plasma-activated deionized water and normal saline.

53 species and 624 chemical reactions are incorporated. The densities of species are obtained by calculating the plasma chemistry, the particle fluxes between the plasma region and the air gap region, and the dissipated power density which should be equal to the set value. In the plasma region, the mass conservation equations are used to calculate the densities of species, as follows[16]:

$$\frac{\partial n_{p,i}}{\partial t} = R_{p,i} - \frac{\Gamma_{pg,i}}{d_p} \tag{1}$$

where $n_{p,i}$ stands for the density of ith species in the plasma, $R_{p,i}$ represents the sum of the reaction rates, $\Gamma_{pg,i}$ is the particle flux between the plasma region and the air gap region, and d_p is the thickness of the plasma region which is set to be 100 µm based on the typical radius of discharge filaments. The power density is calculated based on the electric field strength, which is estimated by a Gaussian-like pulsed profile as detailed in ref. [16]

There is an air gap region with a width of 1 cm between the plasma region and the liquid region. Only neutral species are considered in the air gap region, so the number of the species and the corresponding reactions are reduced to 21 and 63, respectively. The diffusion and chemical reactions of the neutral species in the air gap, as well as their boundary fluxes on the plasma-gas and gas-liquid interfaces, are calculated by a one-dimensional module. The governing equation of the air gap region is as follows:

$$\frac{\partial n_{g,i}}{\partial t} - D_{g,i} \nabla^2 n_{g,i} = R_{g,i} \tag{2}$$

where $n_{g,i}$ represents the density of ith species, $D_{g,i}$ stands for the diffusion coefficient, and $R_{g,i}$ is the sum of reaction rates of ith species.

Henry's law is used to describe the density relationship of species on both sides of the gas-liquid interface. The module for the plasma-activated normal saline is also one-dimensional with a length of 1 cm, which incorporates 58 species and 205 chemical reactions. Due to the heterogeneous hydrolysis or ionization of some species such as N_2O_5, HNO_2, HNO_3, and Cl_2O_3, a weak electric field will be formed at the gas-liquid interface, so in this module drift-diffusion equations for each species and the Poisson's equation for the electric field E are utilized as follows:

$$\frac{\partial n_{l,i}}{\partial t} + \nabla \cdot \left(-D_{l,i} \nabla n_{l,i} + Z_i u_i n_{l,i} E \right) = R_{l,i} \tag{3}$$

$$\frac{\partial E}{\partial t} = \Sigma Z_i n_{l,i} / \varepsilon \tag{4}$$

Table 1. Species considered in the model

Plasma region

Cations $\quad$ N^+, N_2^+, N_3^+, N_4^+, NO^+, N_2O^+, NO_2^+, H^+, H_2^+, H_3^+, O^+, O_2^+, O_4^+, OH^+, H_2O^+, H_3O^+

Anions $\quad$ e, O^-, O_2^-, O_3^-, O_4^-, NO^-, NO_3^-, H^-, OH^-, N_2O^-, NO_2^-

Neutrals $\quad$ $N(^2D)$, $N_2(A^3\Sigma)$, $N_2(B^3\Pi)$, H, N, H_2, N_2, H_2O, $O(^1D)$, O, $O_2(a^1\Delta)$, O_3, OH,

$\qquad$ HO_2, H_2O_2, O_2, NO, NO_2, NO_3, N_2O_3, N_2O_4, N_2O_5, HNO_2, HNO_3, N_2O, HNO

Air gap region $\quad$ NO, N_2O, NO_2, NO_3, N_2O_3, N_2O_4, N_2O_5, HNO, HNO_2, HNO_3, N, N_2, O_2, O, $O_2(a^1\Delta)$, O_3, OH,

$\qquad$ HO_2, H_2O_2, H_2, H_2O

Liquid region

Deionized water $\quad$ O, O_3, OH, HO_2, HO_3, H_2O_2, N_2, O_2, H_2O, H, H_2, N_2O_3, NO, NO_2, NO_3, N_2O_4, N_2O_5, HNO_2,

$\qquad$ H^+, HO_2^-, OH^-, O^-, O_2^-, O_3^-, NO_2^-, NO_3^-, O_2NOOH, O_2NOO^-, $ONOO^-$, $ONOOH$, HNO_3, N_2O

Normal saline $\quad$ O, O_3, OH, HO_2, HO_3, H_2O_2, N_2, O_2, H_2O, H, H_2, N_2O_3, NO, NO_2, NO_3, N_2O_4, N_2O_5, HNO_2,

$\qquad$ H^+, HO_2^-, OH^-, O^-, O_2^-, O_3^-, NO_2^-, NO_3^-, O_2NOOH, O_2NOO^-, $ONOO^-$, $ONOOH$, HNO_3, N_2O

$\qquad$ HCl, $HClO$, $HOClH$, $HOCl^-$, $HClO_2$, Cl, Cl^-, Cl_2, Cl_2^-, Cl_3^-, ClO^-, ClO, ClO_2^-, ClO_2, ClO_3^-, ClO_3,

$\qquad$ ClO_4^-, Cl_2O, Cl_2O_2, Cl_2O_3, Cl_2O_4, Cl_2O_5, Cl_2O_6, $ClNO_2$, Na^+

where $n_{l,i}$ represents the density of *ith* species in the liquid region, $D_{l,i}$ is the diffusion coefficient, μ_l stands for the mobility of the charged species in water which is calculated by the Stokes-Einstein Relation, $R_{l,i}$ is the sum of aqueous reaction rates, Z_i is the absolute value of the charge, and ε represents the dielectric constant of the liquid.

The commercial software, COMSOL Multiphysics$^{@}$, was adopted to construct this model. Both the lengthes of the air gap and the liquid region are set to be 1 cm, the plasma power density is set to be 0.05 W/cm^2, and the gas temperature is set to be 300 K. The initial gas composition is 76.63% N_2, 20.37% O_2, and 3% H_2O, and the initial densities of other species in the plasma and the air region are set to be 10^{10} m^{-3}. The power density is four times lower than that used for the bactericidal experiments as discussed above, because we want to compare the results with our previous reports of plasma-activated deionized water with the same power density.[16,20] The initial concentrations of Na$^+$ and Cl$^-$ in the normal saline are set to be 0.154 M (mol/L), corresponding to the mass fraction of 0.9%. The initial pH value of the normal saline is set to be 7, which means the concentrations of H$^+$ and OH$^-$ in liquid are 10^{-7} M. The initial concentrations of dissolved O_2 and N_2 are set to be 1.27×10^{-3} and 5.94×10^{-4} M, respectively, by considering their particle balance between the gas and liquid phases. And the initial concentrations of other aqueous species are set to be 10^{10} m^{-3}. Several assumptions were made by

careful consideration. The diffusion of charged species from the plasma into the air gap is neglected, because their diffusion distances in lifetimes are less than 100 μm,[16] and therefore such diffusion has little effect on the remote liquid region which is focused in this paper. The volatilization of some chlorine/oxy-chlorine species (such as Cl$_2$) are neglected because of their low concentrations.

4. Aqueous Reactive Species and Their Chemical Pathways

According to the simulation results, the concentration distributions of RNS and ROS in the normal saline are shown in Figure 3, for the plasma treatment time of 100 s. It can be seen that the dominant ROS are O_3 and H_2O_2, and the dominant RNS are nitrate (HNO_3/NO_3^-), nitrous oxide (N_2O) and nitrite (HNO_2/NO_2^-), which are the same principal constituents as that of the plasma-activated deionized water.[16] Also, various short-lived species
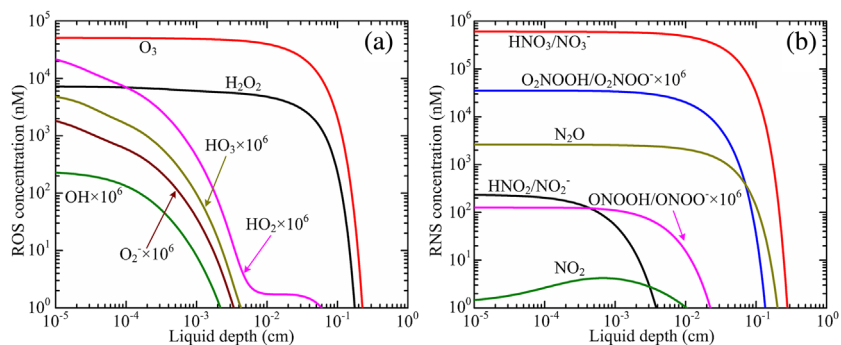
Figure 3. Concentration distributions of ROS (a) and RNS (b) in the plasma-activated normal saline after the plasma treatment of 100 s.

↖ **Early View Publication; these are NOT the final page numbers, use DOI for citation !!**

including OH, O_2^-, HO_2, HO_3, hydroxynitrate (O_2NOOH/O_2NOO^-), and peroxynitrite ($ONOOH$/$ONOO^-$) are found to exist, and these species are mainly generated in situ in the plasma-activated normal saline. The generation mechanism of the short-lived ROS/RNS in the plasma-activated normal saline is very similar to that reported in the plasma-activated deionized water,[20] and hence not discussed here.

Besides the production of ROS and RNS, various kind of reactive chlorine/oxy-chlorine species (RCS) are also generated in normal saline, and their concentration distributions are shown in Figure 4 after the different plasma-on time of 1, 10, and 100 s. In general, the concentrations of all RCS increase with the plasma treatment time. Hypochlorite ($HClO$/ClO^-) is the dominant RCS, followed by Cl_2. After the plasma-on time of 100 s, the maximum concentration of $HClO$/ClO^- is

Figure 4. Concentration distributions of RCS in the plasma-activated normal saline after a plasma-on time of 1 (a), 10 (b), and 100 s (c).

$\sim$197 μM, larger than the reported minimum bactericidal concentration for *S. aureus* by more than one order of magnitude.[17] At the same time, the maximum concentration of Cl_2 is $\sim$12.2 μM, which may also have strong biological effects because 98% of *S. aureus* have been reported to be killed by 35.2 μM Cl_2.[21] In addition to $HClO$/ClO^- and Cl_2, other RCS also have the strong bactericidal ability. For example, it has been reported that the bactericidal ability of ClO_2 is slightly stronger than Cl_2.[21] However, their average concentrations are too low to have the strong bactericidal effect alone, and they may contribute on the sterilization via synergistic combination with the other species.[22,23]

It should be noted that the pH value of the normal saline decreases with the plasma-on time. It is 4.77 at the plasma-on time of 100 s. This value is slightly higher than that in the plasma-activated deionized water (pH = 4.64 at the plasma-on time of 100 s).[16] Since the pKa value of $HClO$ is 7.54,[24] its ionization (R17, in the Supporting Information) is increasingly restricted with the plasma-on time, and at the plasma-on time of 100 s the concentration ratio of $[ClO^-]$/$[HClO]$ is very small value of 2.14×10^{-4}. So, in aqueous hypochlorite, the number of $HClO$ rather than ClO^- is much more. The consistent decrease of pH value also restricts the hydrolysis of Cl_2 (R1), which is the main reason for the accelerated increase of Cl_2 concentration. The pH value decreases to a lower value than 4 after 100 s of plasma treatment in the surface layer of the solution, where Cl_2 mainly exists (see Figure 4).

As shown in Figure 4, concentration distributions of most RCS have a parabolic shape, and this shape penetrates deeper with the plasma-on time. Taking $HClO$/ClO^- for instance, the penetration speed is almost invariable to be $\sim$18.6 μm/s, which is obtained with the concentration criterion of 1 nM. This speed is similar to that reported for the ROS/RNS in the counterparts of deionized water.[16] The parabolic shape of the concentration distributions is because that the RCS are mainly generated from the reactions involving ROS/RNS, concentrations of which have the parabolic shapes as shown in Figure 3.

Various RCS are generated in the plasma-activated normal saline (see Figure 4), which are originated from the aqueous ROS and RNS. In other words, the generation of RCS must consume lots of ROS and RNS. In order to demonstrate this, we plotted in Figure 5 the concentration distributions of several ROS and RNS in normal saline and deionized water after the same conditions of plasma treatment. It can be seen from Figure 5a that the concentrations of short-lived ROS (OH, O_2^-, and HO_2) in normal saline are lower than that in deionized water by more than two orders of magnitude. This significant decline in concentrations indicates that the short-lived ROS must have strong reactions with the chlorine/oxy-chlorine species. The main reactions are as follows:
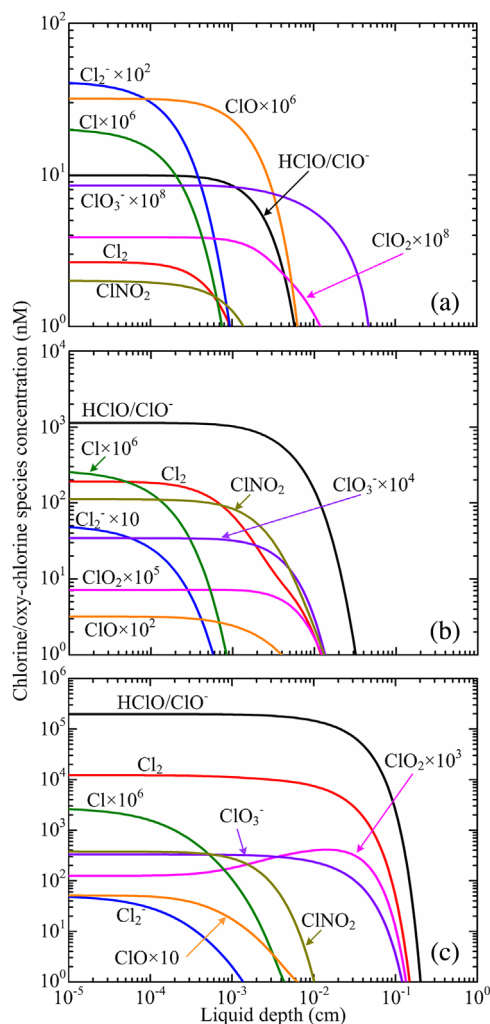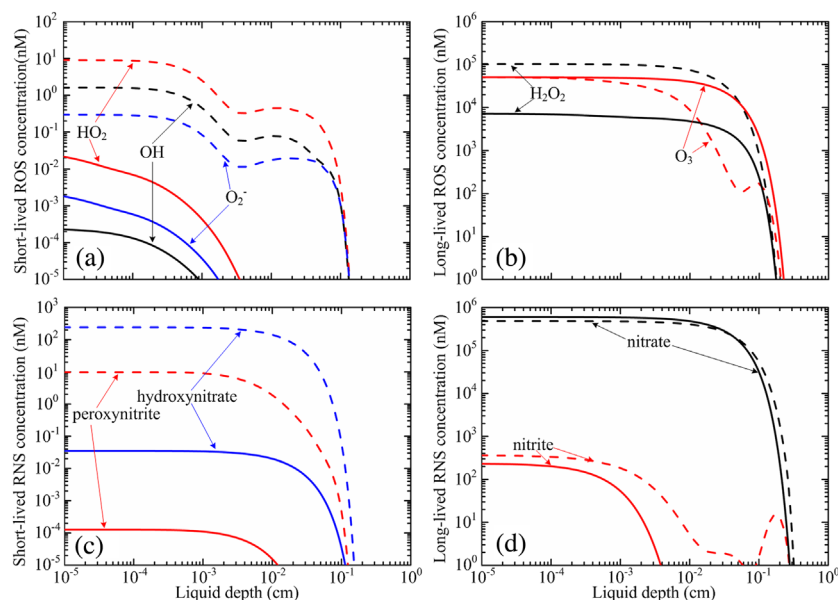
Figure 5. Comparison of the aqueous ROS and RNS in the plasma-activated normal saline and deionized water after 100 s of plasma treatment. The dash lines represent the concentration distributions of species in the plasma-activated deionized water, and the solid lines represent that in the plasma-activated normal saline.

$$Cl^- + OH \rightarrow OH^- + Cl, \tag{R22}$$

$$O_2^- + Cl_2 \rightarrow Cl_2^- + O_2, \tag{R29}$$

$$Cl_2 + HO_2 \rightarrow Cl_2^- + H^+ + O_2. \tag{R28}$$
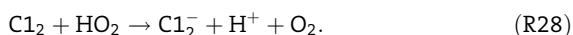
For the long-lived ROS as shown in Figure 5b, the concentration of H_2O_2 in normal saline is lower by $\sim$12.5-fold. However, in contrary, the concentration of O_3 in normal saline is slightly higher. The main reactions for destruction of H_2O_2 by chloride species are as follows:

$$Cl + H_2O_2 \rightarrow Cl^- + H^+ + HO_2, \tag{R26}$$

$$Cl_2^- + H_2O_2 \rightarrow 2Cl^- + H^+ + HO_2, \tag{R35}$$

$$Cl_2^- + H_2O_2 \rightarrow OH + OH^- + Cl_2. \tag{R36}$$
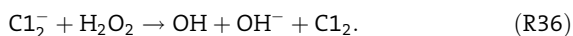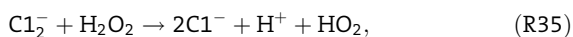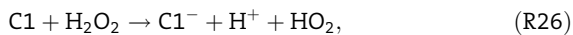
Although these reactions lead to the production of OH and HO_2, the reduction of such two species is even stronger (R22 and R28), and eventually their concentrations lower down.

The higher O_3 concentration in the plasma activated normal saline is due to the lower nitrite (HNO_2/NO_2^-)

concentration as shown in Figure 5d, because the aqueous O_3 is mainly consumed by reacting fastly with NO_2^-: $NO_2^- + O_3 \rightarrow O_2 + NO_3^-$.[20] This reaction is the reason why the front concentration depression of O_3 and the front concentration peak of NO_2^- disappear simultaneously. The lower NO_2^- concentration in the plasma-activated normal saline is due to its reacting with HClO (R60) and Cl_2 (R59), and both reactions result in the production of $ClNO_2$, as follows:

$$Cl_2 + NO_2^- \rightarrow ClNO_2 + Cl^-, \tag{R59}$$

$$HClO + NO_2^- \rightarrow ClNO_2 + OH^-. \tag{R60}$$
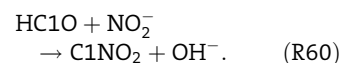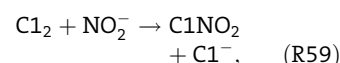
For the short-lived RNS as shown in Figure 5c, peroxynitrite (ONOOH/ONOO$^-$) and hydroxynitrate (O_2NOOH/O_2NOO^-) have their concentrations reduced by more than four orders of magnitude in the plasma-activated normal saline, compared with that in the plasma-activated deionized water.[16] As predicted in our previous report,[20] the short-lived ROS such as OH, O_2^-, and HO_2 play a crucial role in the generation pathways of peroxynitrite and hydroxynitrate. Therefore, the consumption of these short-lived ROS is the main reason for the reduction of these two species concentrations. Moreover, the reaction between hydroxynitrate and Cl$^-$ results in further reduction of the hydorxynitrate concentration, as follows:

$$O_2NOOH + Cl^- \rightarrow HClO + NO_3^-. \tag{R96}$$

In order to validate the simulation results, the concentrations of H_2O_2 were measured in normal saline and deionized water for different durations of plasma treatment, as shown in Figure 6. Here, the average power density used for experiments was 0.05 W/cm^2. The peak value and the frequency of the sinusoidal high-voltage presented above were not changed, but a digital pulse modulator was used with a frequency of 500 Hz and a duty ratio of $\sim$25%. The high-voltage power source was controlled by the digital pulse modulator, and high voltage outputs when the digital signal was "1." A microplate reader (Thermo Scientific Varioskan® Flash Reader) was used for this measurement, and the Amplex® Red reagent was chosen as the indicator of H_2O_2. This indicator was added into the solutions right after the
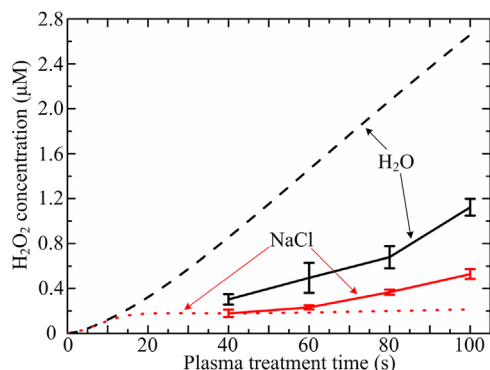
Figure 6. Numerical and experimental data of the spatial-averaged concentrations of H_2O_2 in plasma-activated normal saline and deionized water. The solid fold lines are the experimental results, while the dash curves represent the numerical results.

plasma treatment, and it reacted with H_2O_2 in a 1:1 stoichiometry to produce the red-fluorescent oxidation product, which was excited at $\lambda = 550$ nm and emitted at $\lambda = 595$ nm. The measurements were repeated three times. As shown in Figure 6, the experimental data agrees with the numerical data for the H_2O_2 concentration is higher in the plasma-activated normal saline. In quantitative, the concentration difference between the numerical and experimental data is at most ~2.6-fold for the case of 100 s plasma treatment of normal saline. These agreements indicate that the numerical results are much reliable. It should be noted that Amplex® Red reagent may react with some RCS to produce similar red-fluorescent oxidation product, which would lead to some measuring error. However, since the concentrations of RCS are much lower than that of H_2O_2, this error should have little impact.

We tried to measure more aqueous ROS/RNS including OH and NO using electron spin resonance. However, spin traps used do not react with the target species specifically. For example, DMPO (5, 5-dimethyl-1-pyrrolineN-oxide) is normally used for trapping OH radical, but it also reacts with HClO.[25] Since HClO has higher concentration than OH (see Figures 3 and 4), the measuring error is not acceptable. We also tried to measure the aqueous HClO by colorimetric methods. Aqueous HClO can oxidize DPD (N′-N′-diethyl-p-phenylenediamine) to a pink compound · DPD$^+$, which has two absorption peaks at $\lambda = 510$ and 551 nm. However, DPD can also be oxidized by aqueous ROS such as ozone to generate similar pink compound · DPD$^+$, so this method is not appropriate since the ROS density is high.[26–29] Another indicator, $H_2NCH_2CH_2SO_3H$, can react with HClO to form TauNHCl, which has an absorption maximum at $\lambda = 250$ nm.[30] However, the spectral absorption curve obtained is much different to the typical one as presented in
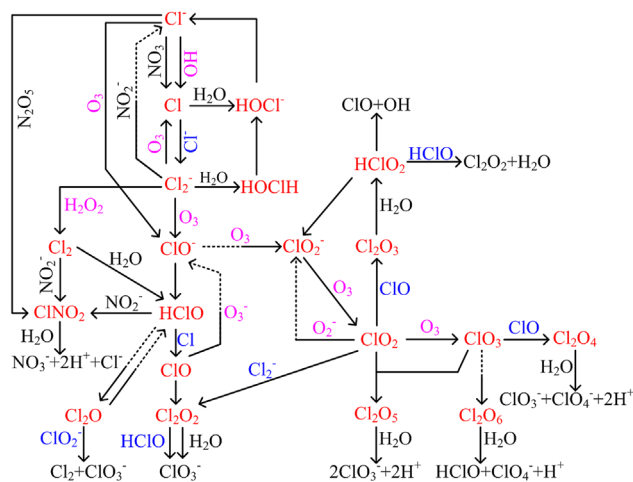
Figure 7. Chemical profile of RCS in normal saline after a plasma-on time of 100 s. The dotted line represents an unimportant pathway while the solid line means important. For example, the reaction between ClO$^-$ and O$_3$ is important for the production of ClO$_2$$^-$ but unimportant for the destruction of ClO$^-$.

ref. [30], indicating that this indicator of HClO is also disturbed by other species in the plasma-activated normal saline.

The chemical profile of RCS in the plasma-activated normal saline is shown in Figure 7, for the plasma-on time of 100 s. Cl$^-$ is certainly the precursor for all the RCS, and it firstly reacts with O$_3$, N$_2$O$_5$, NO$_3$, and OH to form the initial ones (Cl, ClO$^-$, and ClNO$_2$). The main reactions are as follows:

$$\text{C1}^- + \text{O}_3 \rightarrow \text{C1O}^- + \text{O}_2, \qquad (R19)$$

$$\text{C1}^- + \text{OH} \rightarrow \text{OH}^- + \text{C1}, \qquad (R22)$$

$$\text{NO}_3 + \text{C1}^- \rightarrow \text{NO}_3^- + \text{C1}, \qquad (R55)$$

$$\text{N}_2\text{O}_5 + \text{C1}^- \rightarrow \text{C1NO}_2 + \text{NO}_3^-. \qquad (R56)$$

The production rate of ClO$^-$ via R19 is 3.37×10^{17} m^{-3} s^{-1}, the total production rate of Cl via R22 and R55 is 2.54×10^{19} m^{-3} s^{-1}, and it is 1.52×10^{17} m^{-3} s^{-1} for ClNO$_2$. Therefore, the total production rate of RCS is 2.60×10^{19} m^{-3} s^{-1}, and this rate is strongly correlated with the discharge power by which the yield of ROS and RNS is mainly determined. The dominant pathways for the production of the RCS are novel. Taking Cl for example, it is mainly generated by R22, R41, and R55 in the plasma-activated normal saline, but in other cases without the plasma activation the main production way has been reported to be consisted of two stepwise reactions: OH+ Cl$^- \rightarrow$ HOCl$^-$ (R4) and HOCl$^-$ +H$^+ \rightarrow$ Cl + H$_2$O (R5).[31,32]

Early View Publication; these are NOT the final page numbers, use DOI for citation !!

Various RCS are generated from the initial ones (Cl, ClO^-, and $ClNO_2$), and O_3 plays an important role in the chemical pathways. As shown in Figure 7, ClO^- is mainly generated by the ozonization of Cl^- and Cl_2^- (R19 and R41), and then it is stepwise ozonized to form ClO_2^- (R45), ClO_2 (R13), and ClO_3 (R62). Therefore, an important chemical chain exists for the transformation of RCS: Cl^- or $Cl_2^- \rightarrow ClO^- \rightarrow ClO_2^- \rightarrow ClO_2 \rightarrow ClO_3$, and O_3 plays as the intermediate for this chain. The chemical chain reduces O_3 concentration with a rate of $4.45 \times 10^{15}\,m^{-3}\,s^{-1}$, much slowerly than the reaction between NO_2^- and O_3. So, the concentration of O_3 in the plasma-activated normal saline is not lower than that in the plasma-activated deionized water. Instead it is comparatively higher due to the lower concentration of NO_2^-. It should be noted that ClO_2 is an immediate oxy-chlorine species for the production of more oxide species including Cl_2O_4, Cl_2O_4, Cl_2O_5 and Cl_2O_6, and these species will finally hydrolyze to form ClO_3^- and ClO_4^-.

Hypochlorite ($HClO/ClO^-$) is the dominant RCS as shown in Figure 4, and $HClO$ and ClO^- can be regarded as one species since they strongly transform to each other reversibly (R17). Taking $HClO$ and ClO^- as a whole, the main generation pathways are as follows:

$$Cl_2 + H_2O \leftrightarrow H^+ + Cl^- + HClO, \qquad (R1)$$

$$Cl^- + O_3 \rightarrow ClO^- + O_2, \qquad (R19)$$

$$Cl_2^- + O_3 \rightarrow ClO^- + Cl + O_2. \qquad (R41)$$

Among the three reactions above, R41 has the highest rate of $3.77 \times 10^{19}\,m^{-3}\,s^{-1}$, which contributes 67.8% of the hypochlorite production. The reduction of $HClO$ is dominated by reacting with NO_2^- (R60) and Cl (R50).

Cl_2 is an important RCS as discussed above, which is mainly generated by R36 as follows:

$$Cl_2^- + H_2O_2 \rightarrow OH + OH^- + Cl_2. \qquad (R36)$$

The production rate via R36 is $2.17 \times 10^{19}\,m^{-3}\,s^{-1}$. Regarding its reduction, the main reactions are as follows:

$$Cl_2 + H_2O \leftrightarrow H^+ + Cl^- + HClO, \qquad (R1)$$

$$Cl_2 + NO_2^- \rightarrow ClNO_2 + Cl^-. \qquad (R59)$$
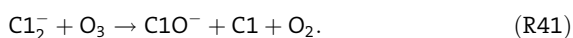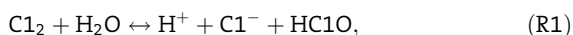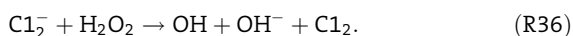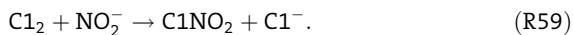
When the pH value is higher than 4, the hydrolysis of Cl_2 (R1) is very fast.[24] However, the pH value in the surface layer of the solution is lower than 4 after 100 s of plasma treatment, and Cl_2 mainly exists in such surface layer as shown in Figure 4. So, Cl_2 can have higher concentration compared to the other RCS.

5. Concluding Remarks

The interaction between a surface air discharge and normal saline is studied in this paper. It is found that the plasma-activated normal saline has a stronger bactericidal effect than that of the plasma-activated deionized water under the same condition. This is surprising and novel since normal saline provides a better living environment for *S. aureus* N315. A model is developed for the whole objects of plasma-liquid interaction including plasma, air and liquid regions, from which the density distributions of aqueous reactive species are presented, and the chemical kinetics of the reactive species are elucidated. Various kinds of reactive chlorine/oxy-chlorine species (RCS) are found to be generated after plasma activation, of which the dominant one is HClO, followed by Cl_2. Such two species reach the minimum bactericidal concentrations as reported in the literature. Regarding the production mechanism of the RCS, Cl^-, is certainly the precursor which firstly reacts with O_3, N_2O_5, NO_3, and OH to form the initial ones (Cl, ClO^-, and $ClNO_2$). Then, the initial RCS further react with the ROS/RNS and themselves to transform to other kinds of RCS, and O_3 plays as an important intermediate in the transformation pathways. The production of RCS reduces the concentrations of ROS/RNS by comparing with that in the plasma-activated deionized water, because a large amount of ROS/RNS is consumed by reacting with the chlorine/oxy-chlorine species. Compared to the plasma-activated deionized water, the ROS/RNS concentrations are lower, but the bactericidal effect is higher in the plasma-activated normal saline, implying that the RCS play a crucial role for the sterilization.

[1] M. G. Kong, G. Kroesen, G. Morfill, T. Nosenko, T. Shimizu, J. van Dijk, J. L. Zimmermann, *New J. Phys.* **2009**, *11*, 115012.
[2] D. Xu, D. Liu, B. Wang, C. Chen, Z. Chen, D. Li, Y. Yang, H. Chen, M. G. Kong, *PLoS ONE* **2015**, *10*, e0128205.

↖ Early View Publication; these are NOT the final page numbers, use DOI for citation !!

[3] S. Y. Zhong, Y. Y. Dong, D. X. Liu, D. H. Xu, S. X. Xiao, H. L. Chen, M. G. Kong, *Br. J. Dermatol.* **2016**, *174*, 542.

[4] M. L. Parisi, E. Fatarella, D. Spinelli, R. Pogni, R. Basosi, *J. Clean. Prod.* **2015**, *108*, 514.

[5] P. Novak, T. Zuliani, R. Milačič, J. Ščančar, *Anal. Chim. Acta* **2016**, *915*, 27.

[6] D. Mariotti, J. Patel, V. Švrček, P. Maguire, *Plasma Process. Polym.* **2012**, *9*, 1074.

[7] D. Mariotti, R. M. Sankaran, *J. Phys. D: Appl. Phys.* **2011**, *44*, 174023.

[8] P. Rumbach, D. M. Bartels, R. M. Sankaran, D. B. Go, *Nat. Commun.* **2015**, *6*, 7248.

[9] W. Tian, M. J. Kushner, *J. Phys. D: Appl. Phys.* **2014**, *47*, 165201.

[10] A. Tani, Y. Ono, S. Fukui, S. Ikawa, K. Kitano, *Appl. Phys. Lett.* **2012**, *100*, 254103.

[11] C. Chen, D. X. Liu, Z. C. Liu, A. J. Yang, H. L. Chen, G. Shama, M. G. Kong, *Plasma Chem. Plasma Process.* **2014**, *34*, 403.

[12] P. Olszewski, J. F. Li, D. X. Liu, J. L. Walsh, *J. Hazard. Mater.* **2014**, *279*, 60.

[13] D. B. Graves, *J. Phys. D: Appl. Phys.* **2012**, *45*, 263001.

[14] S. Samukawa, M. Hori, S. Rauf, K. Tachibana, P. Bruggeman, G. Kroesen, J. C. Whitehead, A. B. Murphy, A. F. Gutsol, S. Starikovskaia, *J. Phys. D: Appl. Phys.* **2012**, *45*, 253001.

[15] M. Witzke, P. Rumbach, D. B. Go, R. M. Sankaran, *J. Phys. D: Appl. Phys.* **2013**, *46*, 129601.

[16] Z. C. Liu, D. X. Liu, C. Chen, D. Li, A. J. Yang, M. Z. Rong, H. L. Chen, M. G. Kong, *J. Phys. D: Appl. Phys.* **2015**, *48*, 495201.

[17] F. D. Pope, J. C. Hansen, K. D. Bayes, R. R. Friedl, S. P. Sander, *J. Phys. Chem. A* **2007**, *111*, 4322.

[18] Y. Sun, Y. Zhang, Y. Xia, T. Fan, M. Xue, Bulgan Enkhbayar, C. Harnoode, A. Dong, *LWT — Food Sci. Technol.* **2014**, *59*, 1068.

[19] L. Wang, M. Bassiri, R. Najafi, K. Najafi, J. Yang, B. Khosrovi, W. Hwong, E. Barati, B. Belisle, C. Celeri, M. Robson, *J. Burns Wounds* **2007**, *6*, 65.

[20] D. X. Liu, Z. C. Liu, C. Chen, A. J. Yang, D. Li, M. Z. Rong, H. L. Chen, M. G. Kong, *Sci. Rep.* **2016**, *6*, 23737.

[21] J. Huang, L. Wang, N. Ren, F. Ma, Juli, *Water Res.* **1997**, *31*, 607.

[22] S. Ikawa, K. Kitano, S. Hamaguchi, *Plasma Process. Polym.* **2010**, *7*, 33.

[23] M. Naïtali, G. Kamgang-Youbi, J. M. Herry, M. N. Bellon-Fontaine, J.-L. Brisset, *Appl. Environ. Microbiol.* **2010**, *76*, 7662.

[24] M. Deborde, U. von Gunten, *Water Res.* **2008**, *42*, 13.

[25] B. M. R. Bandara, O. Hinojosa, C. Bernofsky, *J. Org. Chem.* **1994**, *59*, 1642.

[26] S. Gokulakrishnan, A. Mohammed, H. Prakash, *Chem. Eng. J.* **2016**, *286*, 223.

[27] W. Wang, L. Zhang, T. An, G. Li, H.-Y. Yip, P.-K. Wong, *Appl. Catal. B: Environ.* **2011**, *108–109*, 108.

[28] H. Bader, J. Hoigné, *Water Res.* **1981**, *15*, 449.

[29] W. J. Cooper, N. M. Roscher, R. A. Slifker, *J. Am. Water Works Ass.* **1982**, *74*, 362.

[30] C. R. Chinake, R. H. Simoyi, *J. Phys. Chem. B* **1997**, *101*, 1207.

[31] X.-Y. Yu, J. R. Barker, *J. Phys. Chem. A* **2003**, *107*, 1313.

[32] B. Rao, T. A. Anderson, A. Redder, W. A. Jackson, *Environ. Sci. Technol.* **2010**, *44*, 2961.

[33] W. Behnke, C. George, V. Scheer, C. Zetzsch, *J. Geophys. Res.* **1997**, *102*, 3795.

[34] N. Lahoutifard, P. Lagrange, J. Lagrange, *Chemosphere* **2003**, *50*, 1349.

[35] A. Frenzel, V. Scheer, R. Sikorski, C. George, W. Behnke, C. Zetzsch, *J. Phys. Chem. A* **1998**, *102*, 1329.

[36] D. W. Margerum, L. M. Schurter, J. Hobson, E. E. Moore, *Environ. Sci. Technol.* **1994**, *28*, 331.

[37] H. Herrmann, B. Ervens, H.-W. Jacobi, R. Wolke, P. Nowacki, R. Zellner, *J. Atmos. Chem.* **2000**, *36*, 231.

[38] E. M. Knipping, D. Dabdub, *J. Geophys. Res.* **2002**, *107*, ACH 8–1.

[39] X.-Y. Yu, *J. Phys. Chem. Ref. Dat.* **2004**, *33*, 747.

[40] M. L. Alegre, M. Geronés, J. A. Rosso, S. G. Bertolotti, A. M. Braun, D. O. Mártire, M. C. Gonzalez, *J. Phys. Chem. A* **2000**, *104*, 3117.

[41] N. Kang, W. A. Jackson, P. K. Dasgupta, T. A. Anderson, *Sci. Total Environ.* **2008**, *405*, 301.

[42] T. R. Chigwada, E. Chikwana, R. H. Simoyi, *J. Phys. Chem. A* **2005**, *109*, 1081.

[43] A. K. Horváth, I. Nagypál, G. Peintler, I. R. Epstein, K. Kustin, *J. Phys. Chem. A* **2003**, *107*, 6966.

[44] T. Lundström, H. Christensen, K. Sehested, *Radiat. Phys. Chem.* **2001**, *61*, 109.

[45] L. Deguillaume, K. V. Desboeufs, M. Leriche, Y. Long, N. Chaumerliac, *Atmos. Pollut. Res.* **2010**, *1*, 220.

[46] S. N. Pandis, J. H. Seinfeld, *J. Geophys. Res.* **1989**, *94*, 1105.

[47] G. V. Buxton, C. L. Greenstock, W. P. Helman, A. B. Ross, *J. Phys. Chem. Ref. Dat.* **1988**, *17*, 513.

[48] P. Neta, R. E. Huie, A. B. Ross, *J. Phys. Chem. Ref. Dat.* **1988**, *17*, 1027.

[49] U. von Gunten, *Water Res.* **2003**, *37*, 1469.

[50] R. C. Dunn, J. D. Simon, *J. Am. Chem. Soc.* **1992**, *114*, 4856.

[51] S. L. Quiroga, L. J. Perissinotti, *J. Photoch. Photobio. A* **2005**, *171*, 59.

[52] I. Fabian, G. Gordon, *Inorg. Chem.* **1992**, *31*, 2144.

[53] G. V. Buxton, M. S. Subhani, *J. Chem. Soc. Faraday Trans.* **1972**, *68*, 947.

[54] M. J. Evans, D. J. Jacob, E. Atlas, C. A. Cantrell, F. Eisele, F. Flocke, A. Fried, R. L. Mauldin, B. A. Ridley, B. Wert, R. Talbot, D. Blake, B. Heikes, J. Snow, J. Walega, A. J. Weinheimer, J. Dibb, *J. Geophys. Res.* **2003**, *108*.

Early View Publication; these are NOT the final page numbers, use DOI for citation !!